Showcasing the joint collaborative work from the laboratories of Professor Pritam Mukhapadhayay, Professor Jyotishman Dasgupta and Professor Ayan Datta in India.

A highly contorted push–pull naphthalenediimide dimer and evidence of intramolecular singlet exciton fission

Singlet fission is a photophysical process by which two triplet excitons can be generated in organic chromophores at the cost of one absorbed photon. However only a few classes of chromophores which have triplet energies half the singlet energy can successfully host singlet fission. Here we show for the first time that napthalenediimide (NDI) whose triplet energies do not satisfy this criteria, can still harvest triplets via singlet fission due to the construction of a highly contorted novel NDI dimer.

ROYAL SOCIETY OF CHEMISTRY

rsc.li/chemical-science

Check for updates

A highly contorted push–pull naphthalenediimide dimer and evidence of intramolecular singlet exciton fission†

Deepak Bansal, ‡[a] Arup Kundu, ‡[b] Vijay Pal Singh,[a] Arun K. Pal, [c]
Ayan Datta, *[c] Jyotishman Dasgupta *[b] and Pritam Mukhopadhyay *[a]

Singlet fission is a process by which two molecular triplet excitons are generated subsequent to the absorption of one photon. Molecules that enable singlet fission have triplet state energy at least half of the bright singlet state energy. This stringent energy criteria have challenged chemists to device new molecular and supramolecular design principles to modulate the singlet–triplet energy gap and build singlet fission systems from a wide range of organic chromophores. Herein, we report for the first time intramolecular singlet fission in the seminal naphthalenediimide (NDI) scaffold constrained in a push–pull cyclophane architecture, while individually the NDI chromophore does not satisfy the energy criterion. The challenging synthesis of this highly contorted push–pull cyclophane is possible from the preorganized pincer-like precursor. The special architecture establishes the shortest co-facial NDI⋯NDI contacts (3.084 Å) realized to date. Using broadband femtosecond transient absorption, we find that the correlated T–T pair forms rapidly within 380 fs of photoexcitation. Electronic structure calculations at the level of state-averaged CASSCF (ne,mo)/XMCQDPT2 support the existence of the multi-excitonic T–T pair state, thereby confirming the first example of singlet exciton fission in a NDI scaffold.

Introduction

Multiexciton generation in photostable molecular systems shows promise as a creative route to increase the efficiency of light-energy conversion devices. In the past decade, chemists have successfully demonstrated the generation of two triplet excitons upon photoexcitation in certain classes of pi-conjugated organic chromophores through a process called singlet exciton fission.[1–4] In singlet fission (SF), the energy of the photogenerated singlet excited state gets redistributed with a neighbouring electronically coupled chromophore, *via* an intermediate multi-excitonic state called the correlated triplet–triplet (T–T) pair state,[4] to generate two excited molecules in their independent triplet state. SF as a concept has been successfully exploited by the photovoltaic community to generate solar cells with efficiency higher than the theoretical maxima as calculated by Shockley and Queisser.[5–8] However,

expanding the limited number of successful chromophores for SF to a generic library is a major challenge,[9] principally due to two reasons. Firstly, the molecule has to satisfy an energy criterion,[1] which says that the first excited state singlet energy in the molecule should be greater/equal to twice of the triplet energy, *i.e.*, $E(S_1) \geq 2E(T_1)$. Apart from the singlet-triplet energy requirement, it is necessary to tune the electronic coupling for these chromophores such that SF becomes the fastest mode of excited singlet state decay, thereby maximizing the quantum yield of triplets to be 200%.

Intermolecular SF has been the predominant mechanism for multiexciton generation within molecular crystals and self-assembled molecular aggregates, and therefore prominently exploited in functional devices.[10–15] As such, strong electronic coupling in the excited state within adjacent molecules is the key, which is dependent on noncovalent interactions such as π–π stacking, dipole or van der Waals forces that can proliferate and sustain long-range order.[16] Recently seminal work by Campos and co-workers demonstrated that intramolecular SF in acene dimers can serve to benchmark the spatial dependence of electronic coupling and the interactions that favour ultrafast SF.[13] Subsequently, different acene chromophores were covalently connected through rigid[17–21] or flexible[15] linkers to suitably control the distance and interchromophore orientation for successful intramolecular SF. It is observed that in all these molecular dimers that show SF the correlated T–T pair never dissociates to form free triplets due to fast recombination

aSchool of Physical Sciences, Jawaharlal Nehru University, New Delhi 110067, India. E-mail: m_pritam@mail.jnu.ac.in

bDepartment of Chemical Sciences, Tata Institute of Fundamental Research, Mumbai 400005, India. E-mail: dasgupta@tifr.res.in

cSchool of Chemical Sciences, Indian Association for the Cultivation of Science, Kolkata 700032, West Bengal, India. E-mail: spad@iacs.res.in

† Electronic supplementary information (ESI) available. CCDC 2171334 and 2171335. For ESI and crystallographic data in CIF or other electronic format see https://doi.org/10.1039/d2sc04187a

‡ D. B. and A. K. contributed equally to this work.

arising from the close proximity of the two chromophores. Apart from the covalent interactions in a dimer, it has been realized that molecular strain or backbone distortion in π-conjugated systems can be used to tune the S_1 and T_1 state energies to satisfy the SF energy criterion.[22–25] This idea potentially can allow chromophores which do not satisfy the requisite SF energy criterion to be used as a SF layer in functional photovoltaic devices.

Napthalenediimide (NDI) and its derivatives are versatile photostable chromophores.[26–35] The NDI scaffold has been diversely functionalized to modulate its excited state dynamics, establish artificial light-harvesting, and explore as conduits for electron and energy transfer as well as towards intriguing emissive systems. Recently, phosphorescence as well as delayed fluorescence was observed for the first time from the NDI scaffold.[33,34] In addition, thermally activated delayed fluorescence (TADF) has also been discerned with the NDI scaffold.[35] Importantly, NDI has an unfavourable singlet–triplet (S–T) gap for SF.[36–38] The singlet state energies range from 2.5 eV to 3.5 eV, while triplets can be as high as 2 eV. As a result of this unfavourable S–T gap, SF has not been demonstrated from the NDI scaffold to date.

In our design, we envisaged that maximum electronic communication between the NDI units can be enforced in a cyclophane framework having very close co-facial contacts, which can allow for favourable evolution to the T–T pair state. The key to establishing such close contacts is stitching the NDI units from their core-/short-axis, compared to the synthetically less challenging cyclization from the axial-/long-axis.[39] We therefore predicted significant inward arching of the naphthalene rings in the NDI units when rigid linkers like 1,2-diaminocyclohexane are integrated in the cyclophane framework (Scheme 1). Also, the integration of electron rich donor groups at the core positions of the electron deficient NDI will endow the cyclophane with a push–pull character. Herein, we report the synthesis of a highly contorted cyclophane constructed by fusing diamino linkers at the core positions of two NDI units, and having the shortest co-facial NDI···NDI contacts realized to date. We demonstrate ultrafast intramolecular SF in 380 fs in this novel NDI dimer, thereby providing the first report of a NDI scaffold hosting a T–T pair state.
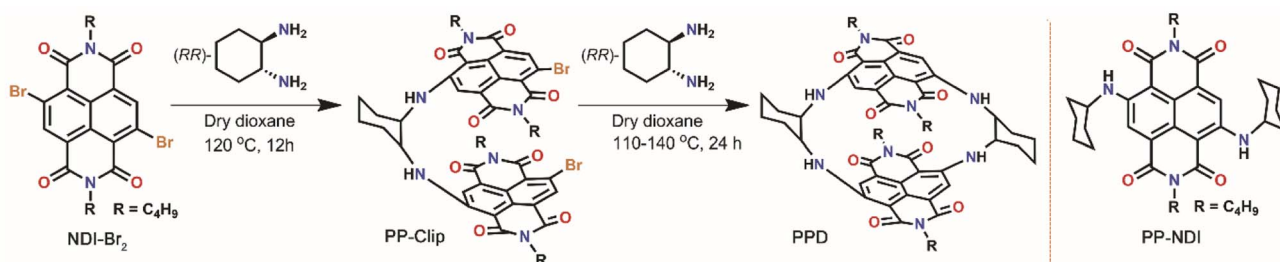
Results and discussion

Synthesis and characterization of PPD

The NDI-dimer **PPD** was synthesized by reacting *N,N*-dibutyl-2,3-dibromo-naphthalene-1,4,5,8-tetracarboxylicacid-bis-imide (**NDI-Br₂**) with (*RR*)-*trans*-1,2-cyclohexanediamine in a stepwise manner (Scheme 1). The challenging aspect of bringing the two electron-rich naphthalene units has been possible from the preorganized **PP-Clip** with a pincer-like architecture. Notably, this is the first example of a NDI cyclophane with donors substituted at the NDI-core and having a push–pull construct. The reference push–pull compound **PP-NDI** was synthesized from **NDI-Br₂**.[40] The synthesis of these compounds was confirmed by different spectroscopic techniques as well as by single crystal X-ray crystallography (Fig. S1–S7, ESI†). Interestingly, ^{1}H NMR of **PPD** exhibits a peak corresponding to the NDI-core H's at 7.90 ppm, which is shielded by 0.25 ppm in comparison to **PP-NDI** (Fig. S3 and S6†). This clearly indicates that the naphthalene rings in **PPD** have developed a significant electron-rich character as a result of the co-facial stacking interactions (*vide infra*) compared to **PP-NDI**.

In addition, from electrochemical studies we observed four distinct electron reduction and four oxidation waves at distinct potentials suggesting strong electronic communication between the NDI units (Fig. S8†). The oxidation and reduction potentials of **PPD** shift towards less positive and more negative values, respectively, compared to **PP-NDI**. This indicates the electron-rich nature of **PPD** and hence easier electron release from the cyclophane.

To have an insight into the structural aspects of **PPD**, we obtained single crystals by slow evaporation of its solution in chloroform–hexane. The crystal structure of **PPD** (see Table S5†) revealed highly contorted, co-facially stacked NDI units with maximal inward arching at the C atoms of the naphthalene rings bonded to the amino groups of cyclohexyldiamine linkers (Fig. 1a). The linkers connect the two NDI units through the alternate C atoms, *i.e.*, C2 of one to C3 of the other NDI unit, while C6 is connected to C7 (Fig. 1b).

These C atoms make the shortest contacts of 3.084 Å and 3.128 Å (Fig. 1b), respectively (calculated using ORTEP-3), which are significantly lower than the sum of the van der Waals radii

Scheme 1 Schematic representation for the synthesis of the NDI core-extended push–pull clip (**PP-Clip**) and push–pull dimer (**PPD**), and structure of the reference molecule **PP-NDI**.
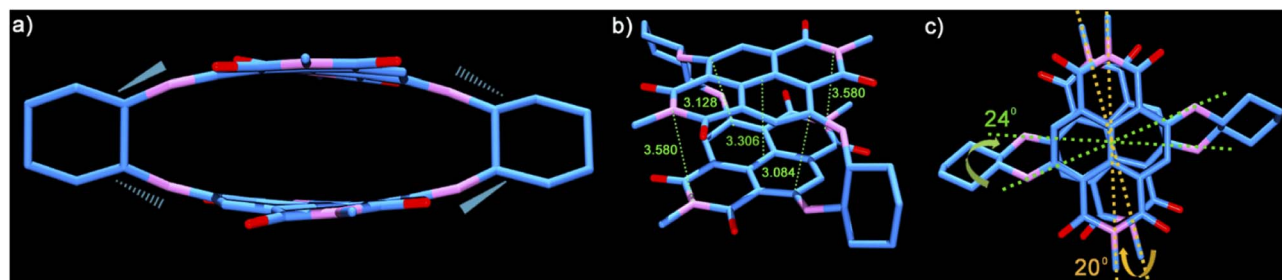
Fig. 1 Single crystal structure of **PPD**. (a) Side view of the push–pull dimer depicting the diagonally positioned above- and below-the-plane cyclohexane (C−N) bonds. (b) Top-frontal view showing the contorted NDI units, the chair conformation of the cyclohexane rings and the various close contacts in Å (calculated using ORTEP-3). (c) Top view showing the slipped NDI π-surfaces and the twisting along the long- and short-axes of **PPD**. The axial *n*-butyl groups and the H atoms have been removed for clarity.

of C atoms (3.4 Å). The central region of **PPD** is arched in an outward fashion with centroid–centroid contacts of 3.306 Å formed between the mid-points of the annular bonds connecting the naphthalene rings. The openings at both the ends of the cyclophane are comparatively wider with the imide N atoms spaced at 3.580 Å. The conformational constraint enforced due to linking the NDI units along its core/short-axis is also evident from the non-eclipsed stacking arrangement of the two π-surfaces (Fig. 1c). The NDI units are twisted by 20° and 24° along the long- and short-axes, respectively (Fig. S9†). Therefore, linking NDI units from their core-/short-axis provides a definite route to realize the shortest contacts between the NDI units in any dimeric construct reported to date and establish a greater contortion of the π-surfaces.[39]

The steady-state absorption spectrum of **PPD** exhibits bands in the regions of 340–440 nm and 450–750 nm with λ_{max} at 600 nm as shown in Fig. 2a. In contrast, **PP-NDI** exhibits bands at 325−420 nm and 450–660 nm due to the π−π* and ICT transitions, respectively (Fig. 2a). Thus, **PPD** exhibits significantly broadened absorption characteristics encompassing the UV and the whole visible region and endows it with a panchromatic character. Fluorescence quenching is observed for **PPD** as compared to its monomer counterpart **PP-NDI**. Notably, the ICT band in **PPD** exhibits a significantly decreased molar extinction coefficient ($\varepsilon_{600} = 5530$ M^{-1} cm^{-1}) compared to that in **PP-NDI**

($\varepsilon_{618} = 27\ 440$ M^{-1} cm^{-1}) suggesting strong electronic coupling between the two co-facially π-stacked NDI units (Fig. S10†). Fig. 2b shows the comparative emission spectrum of **PPD** and **PP-NDI**. **PPD** shows significant quenching in the emission following excitation at 540 nm, suggesting that in the dimer there may be a different non-radiative decay pathway.

Transient absorption spectroscopy

In order to test the feasibility of intramolecular SF in **PPD**, we probed the excited state dynamics of **PPD** with the help of transient absorption spectroscopy and compared it with **PP-NDI**. The excited state dynamics of **PPD** was probed using broadband white light continuum (∼430–1300 nm) subsequent to 400 nm femtosecond pump excitation. Fig. 3a shows the transient absorption spectra of **PPD** at different pump–probe delay time from negative 450 fs to 2 ns in the spectral range of 430 nm to 800 nm. After photoexcitation, we observed two positive excited state absorption (ESA) features centred at ∼500 nm and 740 nm and a negative ground state bleach (GSB) feature in the region of 540 nm to 650 nm. The ESA feature at 500 nm shows an initial rise of 300 fs followed by a monoexponential decay of 68 ps (Fig. 3b). The initial feature at 500 nm is attributed to the absorption of the S$_1$ state. Then it does an internal conversion to another state within the sub-picosecond timescale, which lives for ∼68 ps, as reflected in the single point kinetics at 493 nm, shown in Fig. 3b. On the other hand, the GSB feature at 593 nm shows an initial rise of 2.9 ps, followed by a decay of 66 ps (Fig. 3b and S11†). This concomitant rise in the GSB with the decay of S$_1$ and appearance of another intermediate state is a direct proof of SF in **PPD**. The mismatch in the timescale of the decay of S$_1$ and GSB rise from the single point kinetics analysis is due to the convolution of ESA and GSB features.

To understand the spectral features and the associated lifetimes of different states clearly, we performed singular value decomposition (SVD) analysis of the entire TA spectra of the 430 nm to 800 nm region with a two component sequential model. The normalized Species Associated Spectra (SAS) obtained from the SVD analysis are shown in Fig. 3c. The black trace represents the initially formed S$_1$ state. Within 380 fs, S$_1$ evolves to another state, represented by the red spectrum. The newly formed state could be assigned to a T–T pair state formed
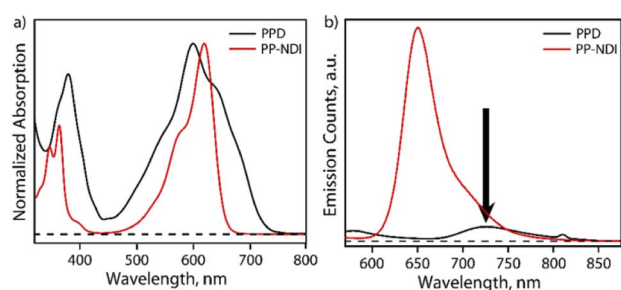

Fig. 2 (a) Steady state absorption spectra of **PPD** (in black) and **PP-NDI** (in red) in DCM at 200 μM concentration, respectively. The **PPD** spectrum shows clear evidence of strong electronic coupling between the NDI scaffolds. (b) Steady state emission spectra of **PPD** (black) and **PP-NDI** (red) in DCM at 200 μM concentration, subsequent to excitation at 540 nm.
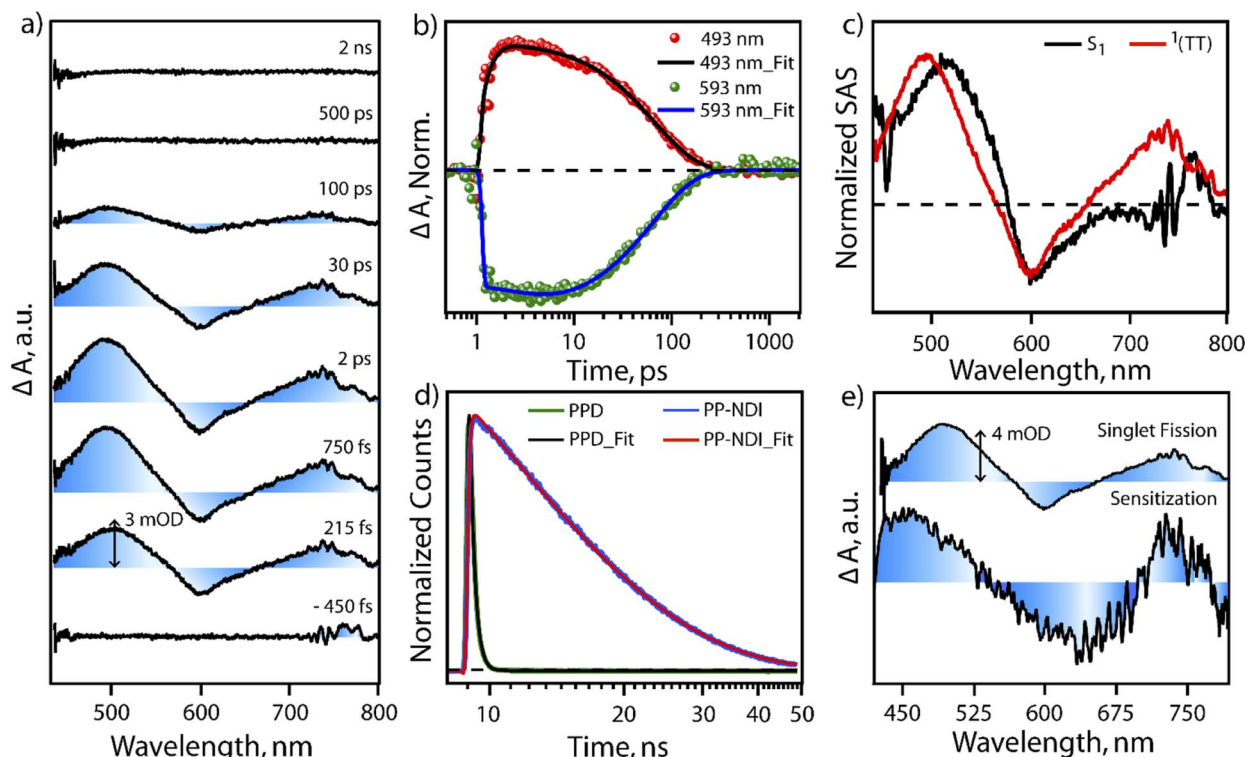
Fig. 3 (a) Transient absorption of **PPD** (100 μM in ACN : DCM (1 : 1)) subsequent to 400 nm photoexcitation. (b) Single point kinetics at 593 nm (GSB) and 493 nm (T−T pair). (c) Normalized species associated spectra followed by two state sequential singular value decomposition of the TA spectra of **PPD**. Black is the S1 state and red is the T−T pair state. (d) TCSPC kinetics data for **PPD** and **PP-NDI**, emission collected at 720 nm, subsequent to excitation at 540 nm. (e) Triplet sensitization measurements of **PPD**. Top: T−T pair spectrum obtained from SF. Bottom: sensitized triplet spectrum of **PPD**.

through SF. This undergoes a fast recombination with a lifetime of 70 ps. In the literature,[41,42] it is well known that triplets formed through intramolecular SF in a dimeric system are prone to rapid recombination due to close proximity. On the other hand, the monomeric NDI derivative (**PP-NDI**) shows a pronounced emissive state that was confirmed using both TCSPC and transient absorption measurements. Fig. 3d shows the fluorescence decay dynamics of the dimer as compared to the monomer with an IRF of ~100 ps by exciting at 540 nm. The data clearly show a lifetime of 10.6 ns for the monomer NDI, while the dimer shows a quenched emission with ~240 ps average lifetime indicative of ultrafast SF. Femtosecond to nanosecond transient absorption spectroscopy on the monomer **PP-NDI** (Fig. S12(a) in ESI†) indicated that the excited state absorption and the stimulated emission spectral features at 470 nm and 650 nm, respectively, lived beyond nanoseconds (Fig. S13†). This clearly indicated that the excited state has a long lifetime, which was quantified precisely using nano-second to microsecond transient absorption spectra (Fig. S12(b)†). The feature at 750 nm was used to ascertain the lifetime to be 10 ns (Fig. S14†). We therefore conclude that the monomer **PP-NDI** is emissive, while the dimer **PPD** shows a non-radiative SF process within 380 fs, dictating the formation of the T−T pair state.

To confirm the formation of the T−T pair state, we performed triplet-sensitization measurements with a Ruthenium sensitizer

mixed in a 2 : 1 concentration ratio with **PPD** (details in the ESI, Fig. S15–S17†). Upon photoexcitation with 400 nm in the mixture, we observe the excited state spectral features of the [Ru-tris(bipy)$_3$]$^{2+}$-complex, which subsequently transfer excitation energy to generate triplets in **PPD**. However, it should be mentioned that we do also see a small fraction of NDI dimer dynamics, which can get triggered due to the overlapping absorption feature at 400 nm by direct photoexcitation (details explained in the ESI†). The NDI dimer dynamics decays within 100 ps, while the Ru-complex displays long-lived excited evolution. On the later timescale, microsecond time region, the Ru-complex does triplet energy transfer to the unexcited **PPD** molecules and a sensitized triplet is formed on the **PPD** molecule. Fig. 3e shows the spectral comparison of the SF induced triplet in **PPD** and the sensitized triplet on the NDI unit in one half of the dimer (**PPD**). It is clearly seen that the ESA features between 450 nm to 525 nm and 700 nm to 750 nm in the sensitized triplet spectra match well with the T−T pair spectra for the **PPD** photoexcitation. It is to be noted that we do not find any evidence for any other non-radiative pathways like symmetry breaking charge separation.[43,44] The radical cation/anion signatures of NDI were not observed in our case. We therefore conclude that **PPD** does produce T−T species, which are weakly coupled to show almost similar spectra as the free triplet that can be hosted on the dimer. Also, our pump excitation wavelength dependent study following excitation at

620 nm in the ICT transition band shows similar spectral features (with better signal/noise) and timescales for SF in **PPD**. We do note that the lifetime of the T–T pair state is longer for the 620 nm excitation indicating that the detection of SF is more sensitive when exciting at 620 nm due to the larger extent of photoexcitation. We therefore infer that excitation at $\pi–\pi^*$ and the ICT band lead to the same T–T pair formation in **PPD** through the SF mechanism.

Electronic structure calculations

The multiexciton (ME) state in a SF process *i.e.* the correlated T–T pair state is a doubly excited state and hence, a single reference method such as TDDFT cannot properly describe this state. For that reason, we have employed static correlated SA3-CASSCF along with the dynamic correlated XMCQDPT2 method. The excitation energies for the ME state formally designated in computations as the lowest singlet excited state S_{1a} (T–T state) while the first optically allowed singlet excited state (ICT) is designated as S_{2a} are listed in Table 1.

An equal weightage of the ground state and excited states was used to configure the wavefunctions for SA3-CASSCF calculations, where we have used C_1 point group symmetry (computational details are provided in the ESI†). The S_{2a} state is optically active as it carries the local excitation (LE) and charge transfer (CT) characters. The dark state which is 0.6 eV lower in energy with respect to the S_{2a} state has an ME character and therefore leads to an exoergic singlet fission. The excitation energies for the S_{1a} and S_{2a} states increase with the increase in CAS active space and active orbitals. For instance, 2.63 eV is the energy for the S_{2a} state with SA3-CAS(4,4), whereas it is 2.90 eV for the SA3-CAS(10,10) calculations.

From this observation, it is obvious that low-lying singlet excited states are well defined by HOMO-to-LUMO and HOMO−1-to-LUMO+1 transitions and the frontier molecular orbitals further lower in energies were treated as a rigid core.[45,46] Therefore, in such cases, the active space requirement in SA-CAS beyond 4e–4o is not effective. However, we also performed CAS(12,10)/NEVPT2/def2-SVP calculations that predict the energy of the optically active excited singlet state as 2.13 eV, which is close to the experimental value (1.80 eV). The configuration state functions corresponding to the S_{1a} and S_{2a} states are shown in Table S1 of the ESI,† where the spin arrangements in ME, LE and CT states are also captured. The molecular orbital diagrams for the ME, LE and CT states are shown in Fig. 4. These calculations confirm the existence of a ME state close in energy to the LE with a highly mixed CT character.

Fig. 4 The molecular orbital (isovalues of ±0.04 au) corresponding to the ME configuration in the S_{1a} (dark) state and LE and CT configurations in the S_{2a} (bright) state.

Furthermore, the S_1 and T_1 energies for the NDI monomer, *i.e.* **PP-NDI**, show that SF on the monomer backbone is endoergic as $E(2T_1) > E(S_1)$ (Table S2†). Although the NDI monomer backbone does not thermodynamically support SF, we observe that our novel contorted NDI dimer, **PPD**, does allow for exoergic SF. Our observations, the first for the NDI class of molecules, are actually similar to covalently linked perylene diimide (PDI) dimers.[25] However, for PDI dimers, the energy transfer is suppressed by the formation of a low-energy excimer.[47,48] Consequently, Dover *et al.* have systematically explained that the challenging task is to design an endothermic SF material that avoids excimer formation.[49] Therefore, for the present case, it is important to verify whether the formation of the ME state is trapped by an excimer formation or not. The excimer structure is obtained by calculating the energy of the S_{2a} state where the centre-to-centre distance (d, in Å) of the **PPD** dimer is varied from 3.30 Å to 3.80 Å with an interval of 0.02 Å. These calculations are performed by the TDDFT method. The potential energy diagram is shown in Fig. 5, which suggests that the π-stacked structure with $d = 3.50$ Å belongs to the minima. Therefore, we have taken the structure as an excimer and the same procedure has been followed by Gao *et al.*[50] The SA-CAS(4,4)/XMCQDPT2 calculated low-lying singlet excited states for the excimer structure are $S_{1a} = 1.98$ eV (ME) and $S_{2a} = 2.64$ eV (CT + LE), comparable with the values in Table 1. Hence, the S_{2a} minima contain the characteristics of an excimer but do
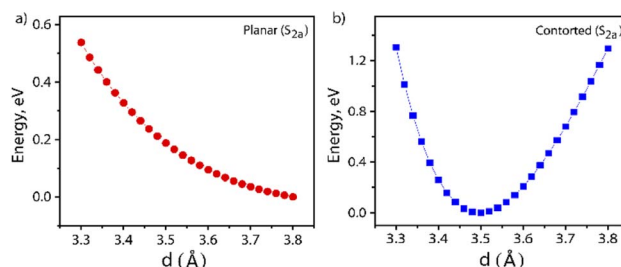
Table 1 Low lying singlet and triplet excitation energies (in eV) of **PPD** using the SA3-CASSCF (n_e, m_o)/XMCQDPT2//DZV level of theory. The characters (χ) of the excited states are also listed

(n_e, m_o)	S_{1a}	χ	S_{2a}	χ	T_1
(4,4)	1.97	ME	2.63	CT + LE	1.84
(6,6)	2.13	ME	2.77	CT + LE	2.05
(8,8)	2.09	ME	2.71	CT + LE	—
(10,10)	2.24	ME	2.90	CT + LE	—

Fig. 5 Potential energy surface plot for the geometry scan of the first excited singlet state (S_{2a}) of: (a) planar and (b) contorted **PPD**. The centre-to-centre distance (d) of 3.50 Å shows the minima for the contorted **PPD**.

not act as a proper excimer, named the excimer-like structure. Such an intermediate before the formation of the ME state generally does not act as a trap and hence increases the triplet yield.[51] The same calculations have been performed for planar **PPD**, where we have removed the bridges in **PPD** and reoptimized it. The dimer makes the two NDI units planar with a stacking distance of 3.49 Å (Fig. S20†). Interestingly, for this case, no such observation is found (see Fig. 5 and Table S3†).

To summarize, the NDI monomers used here have triplet energies that would not satisfy the SF energy criteria. However, by covalent stitching of these monomers in a dimer (**PPD**), we find singlet fission operative on an ultrafast timescale. The multiexcitonic T–T pair state is optimally stabilized in the dimer and avoided an excimer trap as analysed by electronic structure theory. We find that the photoexcitation of the π–π^* (400 nm excitation to S_{3a}) or ICT (620 nm excitation to S_{2a}) features provides an ultrafast access to the multi-excitonic T–T pair state as shown in Fig. S21.† It is known that such excimer traps are also seen in other arylenediimides like PDI where endoergic SF has also been observed (Table S4†).[52–55] This is in contrast to that of terylenediimides, where triplets follow the SF criteria to drive an exoergic SF (Table S4†).[56–58] Our work, therefore, provides a framework for designing new SF systems even when triplet state energies are not ideal for hosting SF.

Conclusion

In conclusion, we have synthesized a new co-facially stacked NDI dimer having the shortest NDI···NDI contacts realized to date, enabling large electronic coupling of the monomer fragments. The short contacts and the contortion in the backbone visualized by the crystal structure of the NDI system allowed for stabilizing a multi-excitonic state, which has a substantial CT character, thereby allowing the excited molecular dimer to channel its excitation energy *via* SF. Therefore, our design enabled the first example of a NDI dimer that shows SF (see the kinetic model in Fig. S21†) within 380 fs due to the inherent backbone contortion. We believe that synthesizing such dimers with varying separation will allow for the optimal understanding and control of SF in NDI dimers. We envision that our exploration will provide a new way of tailoring a new generation of chromophores[59,60] and make them amenable to host SF.

Data availability

Crystallographic data for **PP-NDI** and **PPD** have been deposited at the CCDC under [2171334 and 2171335] and can be obtained from **https://www.ccdc.cam.ac.uk**. The datasets supporting this article have been uploaded as part of the ESI.†

Author contributions

P. M. and D. B. conceived the molecular design. J. D. provided with the experimental methods for measuring the excited state properties. A. D. provided the computational framework for understanding the results. D. B. carried out the synthesis, single crystal X-ray crystallography and electrochemistry experiments. A. K. performed the steady state and transient emission and absorption measurements along with triplet sensitization measurements. A. K. and J. D. analyzed the spectroscopic data. A. K. P. carried out all the theoretical calculations. V. P. S. carried out scaling-up of the product and related spectroscopic characterization. The manuscript was written by P. M., A. K., J. D., A. K. P., A. D. and D. B. The overall discussion and manuscript content was directed by A. D., J. D. and P. M. All the authors agreed to the final version of the manuscript.

Conflicts of interest

There are no conflicts to declare.

Acknowledgements

Notes and references

1 M. B. Smith and J. Michl, *Chem. Rev.*, 2010, **110**, 6891.

2 S. Singh, W. Jones, W. Siebrand, B. Stoicheff and W. Schneider, *J. Chem. Phys.*, 1965, **42**, 330.

3 N. Periasamy and K. Santhanam, *Chem. Phys. Lett.*, 1977, **51**, 442.

4 K. Miyata, F. S. Conrad-Burton, F. L. Geyer and X.-Y. Zhu, *Chem. Rev.*, 2019, **119**, 4261.

5 D. N. Congreve, J. Lee, N. J. Thompson, E. Hontz, S. R. Yost, P. D. Reusswig, M. E. Bahlke, S. Reineke, T. Van Voorhis and M. A. Baldo, *Science*, 2013, **340**, 334.

6 W. Shockley and H. J. Queisser, *J. Appl. Phys.*, 1961, **32**, 510.

7 M. Einzinger, T. Wu, J. F. Kompalla, H. L. Smith, C. F. Perkinson, L. Nienhaus, S. Wieghold, D. N. Congreve, A. Kahn, M. G. Bawendi and M. A. Baldo, *Nature*, 2019, **571**, 90.

8 M. J. Tayebjee, A. A. Gray-Weale and T. W. Schmidt, *J. Phys. Chem. Lett.*, 2012, **3**, 2749.

9 I. Paci, J. C. Johnson, C. Chen, G. Rana, D. Popović, D. E. David, A. J. Nozik, M. A. Ratner and J. Michl, *J. Am. Chem. Soc.*, 2006, **128**, 16546.

10 K. M. Felter and F. C. Grozema, *J. Phys. Chem. Lett.*, 2019, **10**, 7208.

11 A. Kundu and J. Dasgupta, *J. Phys. Chem. Lett.*, 2021, **12**, 1468.

12 A. J. Musser, M. Maiuri, D. Brida, G. Cerullo, R. H. Friend and J. Clark, *J. Am. Chem. Soc.*, 2015, **137**, 5130.

13 E. Busby, J. Xia, Q. Wu, J. Z. Low, R. Song, J. R. Miller, X. Zhu, L. M. Campos and M. Y. Sfeir, *Nat. Mater.*, 2015, **14**, 426.

14 A. J. Musser, M. Al-Hashimi, M. Maiuri, D. Brida, M. Heeney, G. Cerullo, R. H. Friend and J. Clark, *J. Am. Chem. Soc.*, 2013, **135**, 12747.

15 A. Aster, F. Zinna, C. Rumble, J. Lacour and E. Vauthey, *J. Am. Chem. Soc.*, 2021, **143**, 2361.

16 J. C. Johnson, A. J. Nozik and J. Michl, *Acc. Chem. Res.*, 2013, **46**, 1290.

17 S. N. Sanders, E. Kumarasamy, A. B. Pun, M. T. Trinh, B. Choi, J. Xia, E. J. Taffet, J. Z. Low, J. R. Miller and X. Roy, *J. Am. Chem. Soc.*, 2015, **137**, 8965.

18 N. V. Korovina, S. Das, Z. Nett, X. Feng, J. Joy, R. Haiges, A. I. Krylov, S. E. Bradforth and M. E. Thompson, *J. Am. Chem. Soc.*, 2016, **138**, 617.

19 K. Krishnapriya, P. Roy, B. Puttaraju, U. Salzner, A. J. Musser, M. Jain, J. Dasgupta and S. Patil, *Nat. Commun.*, 2019, **10**, 1.

20 N. V. Korovina, J. Joy, X. Feng, C. Feltenberger, A. I. Krylov, S. E. Bradforth and M. E. Thompson, *J. Am. Chem. Soc.*, 2018, **140**, 10179.

21 E. Kumarasamy, S. N Sanders, M. J. Tayebjee, A. Asadpoordarvish, T. J. Hele, E. G. Fuemmeler, A. B. Pun, L. M. Yablon, J. Z. Low and D. W. Paley, *J. Am. Chem. Soc.*, 2017, **139**, 12488.

22 M. Rickhaus, M. Mayor and M. Juríček, *Chem. Soc. Rev.*, 2016, **45**, 1542.

23 K. Nagarajan, A. R. Mallia, V. S. Reddy and M. Hariharan, *J. Phys. Chem. C*, 2016, **120**, 8443.

24 Y. Hong, J. Kim, W. Kim, C. Kaufmann, H. Kim, F. Würthner and D. Kim, *J. Am. Chem. Soc.*, 2020, **142**, 7845.

25 F. S. Conrad-Burton, T. Liu, F. Geyer, R. Costantini, A. P. Schlaus, M. S. Spencer, J. Wang, R. H. Sánchez, B. Zhang, Q. Xu, M. L. Steigerwald, S. Xiao, H. Li, C. P. Nuckolls and X. Zhu, *J. Am. Chem. Soc.*, 2019, **141**, 13143.

26 S. V. Bhosale, M. Al. Kobaisi, R. W. Jadhav, P. P. Morajkar, L. A. Jones and S. George, *Chem. Soc. Rev.*, 2021, **50**, 9845.

27 N. Sakai, R. Bhosale, D. Emery, J. Mareda and S. Matile, *J. Am. Chem. Soc.*, 2010, **132**, 6923.

28 S. Wu, F. Zhong, J. Zhao, S. Guo, W. Yang and T. Fyles, *J. Phys. Chem. A*, 2015, **119**, 4787.

29 A. Aster, C. Rumble, A.-B. Bornhof, H.-H. Huang, N. Sakai, T. Solomek, S. Matile and E. Vauthey, *Chem. Sci.*, 2021, **12**, 4908.

30 H. Kar, D. W. Gehrig, N. K. Allampally, G. Fernández, F. Laquai and S. Ghosh, *Chem. Sci.*, 2016, **8**, 1115.

31 V. L. Gunderson, A. L. Smeigh, C. H. Kim, D. T. Co and M. R. Wasielewski, *J. Am. Chem. Soc.*, 2012, **134**, 4363.

32 S. Kumar, J. Shukla, K. Mandal, Y. Kumar, R. Prakash, P. Ram and P. Mukhopadhyay, *Chem. Sci.*, 2019, **10**, 6482.

33 S. Kuila, K. V. Rao, S. Garain, P. K. Samanta, S. Das, S. K. Pati, M. Eswaramoorthy and S. J. George, *Angew. Chem., Int. Ed.*, 2018, **130**, 17361.

34 S. Kuila, A. Ghorai, P. K. Samanta, R. B. K. Siram, S. K. Pati, K. S. Narayan and S. J. George, *Chem.–Eur. J.*, 2019, **25**, 16007.

35 H. F. Higginbotham, P. Pander, R. Rybakiewicz, M. K. Etherington, S. Maniam, M. Zagorska, A. Pron, A. P. Monkman and P. Data, *J. Mater. Chem. C*, 2018, **6**, 8219.

36 M. Hussain, J. Zhao, W. Yang, F. Zhong, A. Karatay, H. G. Yaglioglu, E. A. Yildiz and M. Hayvali, *J. Lumin.*, 2017, **192**, 211.

37 S. Guo, W. Wu, H. Guo and J. Zhao, *J. Org. Chem.*, 2012, **77**, 3933.

38 S. Wu, F. Zhong, J. Zhao, S. Guo, W. Yang and T. Fyles, *J. Phys. Chem. A*, 2015, **119**, 4787.

39 Y. Wu, M. Frasconi, D. M. Gardner, P. R. McGonigal, S. T. Schneebeli, M. R. Wasielewski and J. F. Stoddart, *Angew. Chem., Int. Ed.*, 2014, **53**, 9476.

40 M. Ajayakumar, D. Asthana and P. Mukhopadhyay, *Org. Lett.*, 2012, **14**, 4822.

41 F. S. Conrad-Burton, T. Liu, F. Geyer, R. Costantini, A. P. Schlaus, M. S. Spencer, J. Wang, R. H. N. Sánchez, B. Zhang and Q. Xu, *J. Am. Chem. Soc.*, 2019, **141**, 13143.

42 S. L. Bayliss, A. D. Chepelianskii, A. Sepe, B. J. Walker, B. Ehrler, M. J. Bruzek, J. E. Anthony and N. C. Greenham, *Phys. Rev. Lett.*, 2014, **112**, 238701.

43 E. Vauthey, *ChemPhysChem*, 2012, **13**, 2001.

44 N. Banerji, A. Fürstenberg, S. Bhosale, A. L. Sisson, N. Sakai, S. Matile and E. Vauthey, *J. Phys. Chem. B*, 2008, **112**, 8912.

45 A. K. Pal, K. Bhattacharyya and A. Datta, *J. Chem. Theory Comput.*, 2019, **15**, 5014.

46 E. A. Buchanan, Z. Havlas and J. Michl, *Adv. Quantum Chem.*, 2017, **75**, 175.

47 K. E. Brown, W. A. Salamant, L. E. Shoer, R. M. Young and M. R. Wasielewski, *J. Phys. Chem. Lett.*, 2014, **5**, 2588.

48 R. E. Cook, B. T. Phelan, R. J. Kamire, M. B. Majewski, R. M. Young and M. R. Wasielewski, *J. Phys. Chem. A*, 2017, **121**, 1607.

49 C. B. Dover, J. K. Gallaher, L. Frazer, P. C. Tapping, A. J. Petty II, M. J. Crossley, J. E. Anthony, T. W. Kee and T. W. Schmidt, *Nat. Chem.*, 2018, **10**, 305.

50 Y. Gao, H. Liu, S. Zhang, Q. Gu, Y. Shen, Y. Ge and B. Yang, *Phys. Chem. Chem. Phys.*, 2018, **20**, 12129.

51 C. M. Mauck, P. E. Hartnett, E. A. Margulies, L. Ma, C. E. Miller, G. C. Schartz, T. J. Marks and M. R. Wasielewski, *J. Am. Chem. Soc.*, 2016, **138**, 11749.

52 N. Renaud and F. C. Grozema, *J. Phys. Chem. Lett.*, 2015, **6**, 360.

53 S. W. Eaton, L. E. Shoer, S. D. Karlen, S. M. Dyar, E. A. Margulies, B. S. Veldkamp, C. Ramanan, D. A. Hartzler, S. Savikhin, T. J. Marks and M. R. Wasielewski, *J. Am. Chem. Soc.*, 2013, **135**, 14701.

54 W. E. Ford and P. V. Kamat, *J. Phys. Chem.*, 1987, **91**, 6373.

55 A. K. Le, J. A. Bender and S. T. Roberts, *J. Phys. Chem. Lett.*, 2016, **7**, 4922.

56 E. A. Margulies, C. E. Miller, Y. Wu, L. Ma, G. C. Schatz, R. M. Young and M. R. Wasielewski, *Nat. Chem.*, 2016, **8**, 1120.

57 X. Zhao, Y. J. Bae, M. Chen, S. M. Harvey, C. Lin, J. Zhou, R. D. Schaller, R. M. Young and M. R. Wasielewski, *J. Chem. Phys.*, 2020, **153**, 244306.

58 E. A. Margulies, J. L. Logsdon, C. E. Miller, L. Ma, E. Simonoff, R. M. Young, G. C. Schatz and M. R. Wasielewski, *J. Am. Chem. Soc.*, 2017, **139**, 663.

59 K. Tajima, K. Matsuo, H. Yamada, S. Seki, N. Fukui and H. Shinokubo, *Angew. Chem., Int. Ed.*, 2021, **25**, 14060.

60 S. Kumar, K. Yoshida, Y. Hattori, T. Higashino, H. Imahori and S. Seki, *Chem. Sci.*, 2022, **13**, 1593.